ICHEP94 Ref. GLS0144 **CLEO CONF 94-7**
Submitted to Pa 16, 2 Pl 9, 19 **July 18, 1994**

Measurement of the Form Factors for $\bar{B}^0 \rightarrow D^{*+}\ell^-\bar{\nu}$

P. Avery,[1] A. Freyberger,[1] J. Rodriguez,[1] S. Yang,[1] J. Yelton,[1] D. Cinabro,[2] T. Liu,[2] M. Saulnier,[2] R. Wilson,[2] H. Yamamoto,[2] T. Bergfeld,[3] B.I. Eisenstein,[3] G. Gollin,[3] B. Ong,[3] M. Palmer,[3] M. Selen,[3] J. J. Thaler,[3] K.W. Edwards,[4] M. Ogg,[4] A. Bellerive,[5] D.I. Britton,[5] E.R.F. Hyatt,[5] D.B. MacFarlane,[5] P.M. Patel,[5] B. Spaan,[5] A.J. Sadoff,[6] R. Ammar,[7] P. Baringer,[7] A. Bean,[7] D. Besson,[7] D. Coppage,[7] N. Copty,[7] R. Davis,[7] N. Hancock,[7] M. Kelly,[7] S. Kotov,[7] I. Kravchenko,[7] N. Kwak,[7] H. Lam,[7] Y. Kubota,[8] M. Lattery,[8] M. Momayezi,[8] J.K. Nelson,[8] S. Patton,[8] R. Poling,[8] V. Savinov,[8] S. Schrenk,[8] R. Wang,[8] M.S. Alam,[9] I.J. Kim,[9] Z. Ling,[9] A.H. Mahmood,[9] J.J. O'Neill,[9] H. Severini,[9] C.R. Sun,[9] F. Wappler,[9] G. Crawford,[10] C. M. Daubenmier,[10] R. Fulton,[10] D. Fujino,[10] K.K. Gan,[10] K. Honscheid,[10] H. Kagan,[10] R. Kass,[10] J. Lee,[10] R. Malchow,[10] M. Sung,[10] C. White,[10] M.M. Zoeller,[10] F. Butler,[11] X. Fu,[11] B. Nemati,[11] W.R. Ross,[11] P. Skubic,[11] M. Wood,[11] M. Bishai,[12] J. Fast,[12] E. Gerndt,[12] R.L. McIlwain,[12] T. Miao,[12] D.H. Miller,[12] M. Modesitt,[12] D. Payne,[12] E.I. Shibata,[12] I.P.J. Shipsey,[12] P.N. Wang,[12] M. Battle,[13] J. Ernst,[13] L. Gibbons,[13] Y. Kwon,[13] S. Roberts,[13] E.H. Thorndike,[13] C.H. Wang,[13] J. Dominick,[14] M. Lambrecht,[14] S. Sanghera,[14] V. Shelkov,[14] T. Skwarnicki,[14] R. Stroynowski,[14] I. Volobouev,[14] G. Wei,[14] P. Zadorozhny,[14] M. Artuso,[15] M. Gao,[15] M. Goldberg,[15] D. He,[15] N. Horwitz,[15] G.C. Moneti,[15] R. Mountain,[15] F. Muheim,[15] Y. Mukhin,[15] S. Playfer,[15] Y. Rozen,[15] S. Stone,[15] X. Xing,[15] G. Zhu,[15] J. Bartelt,[16] S.E. Csorna,[16] Z. Egyed,[16] V. Jain,[16] D. Gibaut,[17] K. Kinoshita,[17] P. Pomianowski,[17] B. Barish,[18] M. Chadha,[18] S. Chan,[18] D.F. Cowen,[18] G. Eigen,[18] J.S. Miller,[18] C. O'Grady,[18] J. Urheim,[18] A.J. Weinstein,[18] M. Athanas,[19] W. Brower,[19] G. Masek,[19] H.P. Paar,[19] J. Gronberg,[20] R. Kutschke,[20] S. Menary,[20] R.J. Morrison,[20] S. Nakanishi,[20] H.N. Nelson,[20] T.K. Nelson,[20] C. Qiao,[20] J.D. Richman,[20] A. Ryd,[20] D. Sperka,[20] H. Tajima,[20] M.S. Witherell,[20] R. Balest,[21] K. Cho,[21] W.T. Ford,[21] D.R. Johnson,[21] K. Lingel,[21] M. Lohner,[21] P. Rankin,[21] J.G. Smith,[21] J.P. Alexander,[22] C. Bebek,[22] K. Berkelman,[22] K. Bloom,[22] T.E. Browder,[22*] D.G. Cassel,[22] H.A. Cho,[22] D.M. Coffman,[22] D.S. Crowcroft,[22] P.S. Drell,[22] D. Dumas,[22] R. Ehrlich,[22] P. Gaidarev,[22] M. Garcia-Sciveres,[22] B. Geiser,[22] B. Gittelman,[22] S.W. Gray,[22] D.L. Hartill,[22] B.K. Heltsley,[22] S. Henderson,[22] C.D. Jones,[22] S.L. Jones,[22] J. Kandaswamy,[22] N. Katayama,[22] P.C. Kim,[22] D.L. Kreinick,[22] G.S. Ludwig,[22] J. Masui,[22] J. Mevissen,[22] N.B. Mistry,[22] C.R. Ng,[22] E. Nordberg,[22] J.R. Patterson,[22] D. Peterson,[22] D. Riley,[22] S. Salman,[22] M. Sapper,[22] and F. Würthwein[22]

(CLEO Collaboration)

[1]*University of Florida, Gainesville, Florida 32611*
[2]*Harvard University, Cambridge, Massachusetts 02138*
[3]*University of Illinois, Champaign-Urbana, Illinois, 61801*
[4]*Carleton University, Ottawa, Ontario K1S 5B6 and the Institute of Particle Physics, Canada*
[5]*McGill University, Montréal, Québec H3A 2T8 and the Institute of Particle Physics, Canada*
[6]*Ithaca College, Ithaca, New York 14850*
[7]*University of Kansas, Lawrence, Kansas 66045*
[8]*University of Minnesota, Minneapolis, Minnesota 55455*
[9]*State University of New York at Albany, Albany, New York 12222*
[10]*Ohio State University, Columbus, Ohio, 43210*
[11]*University of Oklahoma, Norman, Oklahoma 73019*
[12]*Purdue University, West Lafayette, Indiana 47907*
[13]*University of Rochester, Rochester, New York 14627*
[14]*Southern Methodist University, Dallas, Texas 75275*
[15]*Syracuse University, Syracuse, New York 13244*
[16]*Vanderbilt University, Nashville, Tennessee 37235*
[17]*Virginia Polytechnic Institute and State University, Blacksburg, Virginia, 24061*
[18]*California Institute of Technology, Pasadena, California 91125*
[19]*University of California, San Diego, La Jolla, California 92093*
[20]*University of California, Santa Barbara, California 93106*
[21]*University of Colorado, Boulder, Colorado 80309-0390*
[22]*Cornell University, Ithaca, New York 14853*

Abstract

Using a sample of 2.2×10^6 $\Upsilon(4S) \to B\bar{B}$ events collected with the CLEO-II detector at the Cornell Electron Storage Ring, we have measured the form factors for $\bar{B}^0 \to D^{*+}\ell^-\overline{\nu}$. We perform a three-parameter fit to the joint distribution of four kinematic variables to obtain the preliminary form factor ratios $R_1 = 1.30 \pm 0.36 \pm 0.16$ and $R_2 = 0.64 \pm 0.26 \pm 0.12$, and the slope of the Isgur-Wise function, $\rho^2 = 1.01 \pm 0.15 \pm 0.09$. By using the large CLEO data sample and the correlations among the observed kinematic variables, we have measured for the first time all three parameters simultaneously. The form factor ratios are consistent with predicted corrections from the heavy-quark symmetry limit $R_1 = R_2 = 1$. We also present form factor ratios obtained from fits in which ρ^2 is constrained to a series of values. Finally, we observe large effects due to interference terms in the decay rate that are consistent with a $V - A$ coupling at both W vertices.

---

*Permanent address: University of Hawaii at Manoa

I. INTRODUCTION

The decay $B \to D^*\ell\nu$ is a key process for measuring the magnitude of the Cabibbo-Kobayashi-Maskawa (CKM) mixing angle V_{cb} and for testing theoretical predictions of semileptonic decay form factors. These two goals are related, because precise measurements of CKM angles require good predictions for the decay rate. In exclusive processes, such predictions depend on knowledge of form factors, which describe the effect of strong interactions on the underlying weak process. The decay $B \to D^*\ell\nu$ has the largest branching fraction of any semileptonic B decay, and it has very little background. It is therefore well suited experimentally for the detailed studies of kinematic distributions that are required for the measurement of form factors.

The semileptonic decay form factors are Lorentz invariant functions that depend only on q^2, the square of the mass of the virtual W, and their variation is sensitive to nonperturbative QCD interactions. Calculations of charm and bottom semileptonic decay form factors have been based on the quark model [1–3] and, more recently, on lattice QCD methods [4–6] and QCD sum rules [7–10]. A development of major importance is the heavy quark effective theory (HQET) [11]. In the limit of very large quark mass (compared with $\Lambda_{\rm QCD}$), the quark mass and spin decouple from the dynamics of the semileptonic decay, leading to numerous symmetry relations among the form factors. For example, the decay amplitude for $B \to D^*\ell\nu$ involves three form factors (for a massless charged lepton), but heavy-quark symmetry relates all of them to a single form factor, the Isgur-Wise function. Heavy-quark symmetry relations are not as useful when applied to charm semileptonic decay, because the symmetry breaking corrections there are much larger.

Although HQET cannot predict the value of the Isgur-Wise function over the full q^2 range available in the decay, it does predict its value, up to relatively small symmetry breaking and perturbative QCD corrections [12,13], to be unity for the kinematic configuration in which the D^* has zero recoil momentum. In this configuration, the light constituents of the initial meson are nearly undisturbed by the transition from a b to a c quark, since one heavy quark is simply replaced by another. This normalization prediction provides a method to reduce the model dependence in the determination of $|V_{cb}|$, and it has been used by both ARGUS [14] and CLEO [15].

In this analysis, we study the form factors for $\bar{B}^0 \to D^{*+}\ell^-\overline{\nu}$ using the channel $D^{*+} \to D^0\pi^+$ with $D^0 \to K^-\pi^+$ or $D^0 \to K^-\pi^+\pi^0$. We perform an unbinned maximum likelihood fit that incorporates both smearing and acceptance effects by using a Monte Carlo technique [16] to evaluate the likelihood function. The fit provides information on two form factor ratios, defined in the following section, and the slope of the Isgur-Wise function. In contrast to measurements of form factors in charm semileptonic decays, we do not assume pole masses; the slope of the Isgur-Wise function plays the same role as these masses and is determined from the fit. The three-parameter fit is performed using three decay angles (discussed below) and q^2, and it fully incorporates the correlations among these quantities, which provide powerful information not available from the projections only. We have attempted to reduce backgrounds as much as possible so that systematic errors from poorly understood backgrounds such as $B \to D^{**}\ell\nu$ are minimized.

The integrated luminosity of the data sample is 2.04 fb^{-1} on the $\Upsilon(4S)$, which corresponds to $(2.19 \pm 0.02) \times 10^6$ $B\overline{B}$ pairs. We also use a 0.97 fb^{-1} data sample obtained at a center-of-mass energy about 60 MeV below the $\Upsilon(4S)$ to measure the continuum background. The data were collected using the CLEO-II detector, which is described in detail elsewhere [17]. For this analysis, the most important features are the tracking system, which we use to measure charged-pion momenta down to about 60 MeV/c; the CsI calorimeter, which provides excellent photon and electron identification; and the muon system.

II. DECAY DISTRIBUTIONS AND FORM FACTORS FOR $\bar{B}^0 \to D^{*+}\ell^-\overline{\nu}$

The differential decay rate for $\bar{B}^0 \to D^{*+}\ell^-\overline{\nu}$, $D^{*+} \to D^0\pi^+$ can be expressed in terms of three q^2-dependent helicity amplitudes $H_\pm(q^2)$ and $H_0(q^2)$, where the subscripts refer to the helicity of either the virtual W or the D^*. The rate is given by

$$\begin{aligned}\frac{d\Gamma(\bar{B}^0 \to D^{*+}\ell^-\overline{\nu},\ D^{*+} \to D^0\pi^+)}{dq^2\, d\cos\theta_\ell\, d\cos\theta_V\, d\chi} = {} & \frac{3G_F^2|V_{cb}|^2\, P_{D^*}\, q^2}{8(4\pi)^4 m_B{}^2}\mathcal{B}(D^{*+} \to D^0\pi^+) \times \\ & \{[(1-\cos\theta_\ell)^2|H_+(q^2)|^2 + (1+\cos\theta_\ell)^2|H_-(q^2)|^2]\sin^2\theta_V \\ & +4\sin^2\theta_\ell\cos^2\theta_V|H_0(q^2)|^2 \\ & -2\sin^2\theta_\ell\sin^2\theta_V\cos(2\chi)H_+(q^2)H_-(q^2) \\ & -4\sin\theta_\ell(1-\cos\theta_\ell)\sin\theta_V\cos\theta_V\cos\chi\, H_+(q^2)H_0(q^2) \\ & +4\sin\theta_\ell(1+\cos\theta_\ell)\sin\theta_V\cos\theta_V\cos\chi\, H_-(q^2)H_0(q^2)\},\end{aligned} \tag{1}$$

where m_B is the mass of B meson; P_{D^*} is the momentum of the D^* and is a function of q^2; $\mathcal{B}(D^{*+} \to D^0\pi^+)$ is the branching fraction for $D^{*+} \to D^0\pi^+$; and the angles θ_ℓ, θ_V, and χ are defined in Fig. 1. Note that θ_ℓ is defined with respect to the direction of the virtual W; this accounts for the sign differences between our formula and certain others in the literature [2]. The helicity amplitudes $H_\pm$ and H_0 can be expressed in terms of two axial-vector form factors, $A_1(q^2)$ and $A_2(q^2)$, and a vector form factor $V(q^2)$:

$$\begin{aligned}H_\pm(q^2) &= (m_B + m_{D^*})A_1(q^2) \mp \frac{2m_B\, P_{D^*}}{(m_B + m_{D^*})}V(q^2) \\ H_0(q^2) &= \frac{1}{2m_{D^*}\sqrt{q^2}}\Big[(m_B^2 - m_{D^*}^2 - q^2)(m_B + m_{D^*})A_1(q^2) - \frac{4m_B^2\, P_{D^*}^2}{(m_B + m_{D^*})}A_2(q^2)\Big],\end{aligned} \tag{2}$$

where m_{D^*} is the mass of the D^* meson. The form factors A_1, A_2, and V are dimensionless and relatively real, since CP is conserved and there are no final-state strong interactions [2]. We can therefore take them to be real, which is assumed in Eq. 1. As a result of the $V - A$ coupling, the difference $H_+(q^2) - H_-(q^2)$ is typically large and negative.

In the heavy-quark symmetry limit, the form factors are related to the Isgur-Wise function ξ:

$$V(q^2) = A_2(q^2) = A_1(q^2)\left[1 - \frac{q^2}{(m_B + m_{D^*})^2}\right]^{-1} = R^{*-1}\xi(q^2), \tag{3}$$

where $R^* = 2\sqrt{m_B m_{D^*}}/(m_B + m_{D^*}) \approx 0.89$. In this limit, it is more appropriate to write ξ as a function of the quantity

$$w = \frac{m_B^2 + m_{D^*}^2 - q^2}{2m_B m_{D^*}} = \frac{E_{D^*}}{m_{D^*}}. \tag{4}$$

Thus, w is simply the relativistic factor γ for the D^* in the B-meson rest frame. For $\bar{B}^0 \to D^{*+}\ell^-\overline{\nu}$ it ranges from 1 (zero D^* recoil momentum) to about 1.5 (maximum D^* recoil momentum). (The quantity w is sometimes referred to as y in the literature and can also be written as $v \cdot v'$, where v and v' are the four velocities of the initial and final mesons.) For the zero-recoil configuration the value of ξ is determined by heavy quark symmetry:

$$\xi(q^2 = q^2_{max}) = \xi(w = 1) = 1. \tag{5}$$

Following Neubert [10], we define the form factor ratios

$$\begin{aligned} R_1 &\equiv \left[1 - \frac{q^2}{(m_B + m_{D^*})^2}\right] \frac{V(q^2)}{A_1(q^2)} \\ R_2 &\equiv \left[1 - \frac{q^2}{(m_B + m_{D^*})^2}\right] \frac{A_2(q^2)}{A_1(q^2)}, \end{aligned} \tag{6}$$

which are both predicted to be unity in the heavy-quark symmetry limit. However, the b and c quarks are not infinitely heavy, and there are $1/m_b$, $1/m_c$, and α_s corrections. The prediction for the normalization, $\xi(w = 1) = 1$, is protected against $1/m_Q$ corrections by Luke's theorem [12], which states that the leading power corrections arise at order $1/m_Q^2$. There are, however, substantial symmetry breaking effects for the form factor ratios R_1 and R_2. Neubert's estimate of these corrections, which is model dependent, gives

$$R_1 \approx 1.3 \qquad\qquad R_2 \approx 0.8. \tag{7}$$

In fact, both R_1 and R_2 are expected to have a mild q^2 (or w) dependence

$$\begin{aligned} R_1(w) &= 1.35 - 0.22(w-1) + 0.09(w-1)^2 \\ R_2(w) &= 0.79 + 0.15(w-1) - 0.04(w-1)^2. \end{aligned} \tag{8}$$

Since the maximum value of w in $\bar{B}^0 \to D^{*+}\ell^-\overline{\nu}$ is about 1.5, these effects are small, and in our fits we assume that R_1 and R_2 can be taken to be constants. The form factors A_1, A_2, and V can then be written

$$\begin{aligned} A_1(q^2) &= \left[1 - \frac{q^2}{(m_B + m_{D^*})^2}\right] R^{*-1}\xi(w(q^2)) \\ A_2(q^2) &= R_2\, R^{*-1}\xi(w(q^2)) \\ V(q^2) &= R_1\, R^{*-1}\xi(w(q^2)). \end{aligned} \tag{9}$$

Previous studies [14,18] of $B \to D^*\ell\nu$ have fit for different ratios

$$r_V = \frac{V(q^2)}{A_1(q^2)} \qquad\qquad r_2 = \frac{A_2(q^2)}{A_1(q^2)}. \tag{10}$$

These quantities were assumed to be constant in the fits and were reported at $q^2 = q^2_{\rm max}$. However, in the heavy quark symmetry limit, it is not r_V and r_2 that should be approximately independent of q^2, but R_1 and R_2, which is why we have chosen these new variables.

In our fits we assume a linear form for the Isgur-Wise function

$$\xi(w) = 1 - \rho^2(w-1). \tag{11}$$

Although various forms for $\xi(w)$ have been suggested in the literature, the range of w is sufficiently small that most are well approximated by a linear function. Thus, the three parameters measured in the fit are R_1, R_2 and ρ^2.

It is common to report the values of certain other integrated observables that can be derived from the form factors. These are $\bar{A}_{\rm FB}$, the forward-backward asymmetry of the lepton in the W rest frame, and $\bar{A}_{\rm pol}$, which is related to the ratio of longitudinal to transverse polarization of the D^{*+}. They are defined by

$$\bar{A}_{\rm pol} = \frac{2\int P_{D^*} q^2 |H_0|^2 dq^2}{\int P_{D^*} q^2(|H_-|^2 + |H_+|^2) dq^2} - 1 = 2\frac{\Gamma_L}{\Gamma_T} - 1 \tag{12}$$

and

$$\bar{A}_{\rm FB} = \frac{\int_0^1 \frac{d\Gamma}{d\cos\theta_\ell} d\cos\theta_\ell - \int_{-1}^0 \frac{d\Gamma}{d\cos\theta_\ell} d\cos\theta_\ell}{\int_{-1}^1 \frac{d\Gamma}{d\cos\theta_\ell} d\cos\theta_\ell} = \frac{3}{4}\frac{(\Gamma_- - \Gamma_+)}{(\Gamma_L + \Gamma_T)}, \tag{13}$$

where

$$\Gamma_i = \frac{G_F^2 |V_{cb}|^2}{96\pi^3} \int dq^2 P_{D^*} \frac{q^2}{{m_B}^2} |H_i(q^2)|^2, \tag{14}$$

$\Gamma_L = \Gamma_0$, and $\Gamma_T = \Gamma_+ + \Gamma_-$.

The forward-backward asymmetry of the lepton is mainly controlled by R_1, whereas the ratio of longitudinal to transverse polarization is almost completely controlled by R_2. Roughly speaking, R_1 is determined from the $\cos\theta_\ell$ distribution and the $\cos\theta_V$ vs. χ correlation; R_2 is determined from the $\cos\theta_V$ and q^2 distributions; and ρ^2 is determined from the q^2 distribution.

III. EVENT SELECTION AND BACKGROUNDS

The event selection is designed to obtain a signal with low background, so that the systematic errors resulting from the modeling of backgrounds in four dimensions are minimized. Broadly speaking, we select events with at least one electron or muon, a D^{*+} reconstructed in the mode $D^{*+} \to D^0\pi^+$, a D^0 meson reconstructed in either $D^0 \to K^-\pi^+$ or $D^0 \to K^-\pi^+\pi^0$, and kinematics that are consistent with a neutrino recoiling against the $D^{*+}\ell$ system. The D^{*+} signal is observed using the $D^{*+} - D^0$ mass difference to obtain the best resolution. The cuts are similar between the electron and muon channels, and between the $D^0 \to K^-\pi^+$ and $D^0 \to K^-\pi^+\pi^0$ modes, although there are some important differences that we describe below.

The main backgrounds, starting with the largest, are from (1) combinatorial background (fake D^{*+}'s); (2) events in which the D^{*+} and the lepton are not from the same B meson (we call such events uncorrelated D^{*+}–ℓ background because the B mesons are produced nearly at rest, leading to uncorrelated momentum vectors for the D^{*+} and the lepton);

$P_\ell(e)$	$1.0 < P_\ell < 2.45$ GeV/c
$P_\ell(\mu)$	$1.4 < P_\ell < 2.45$ GeV/c
P_{D^0}	< 2.45 GeV/c
P_{π_s}	> 65 MeV/c
$\lvert\Delta M_{D^0}\rvert$ $(K\pi)$	<16 MeV/c^2
$\lvert\Delta M_{D^0}\rvert$ $(K\pi\pi^0)$	<25 MeV/c^2
$\lvert\Delta\delta m\rvert$	<2.0 MeV/c^2
$\lvert\cos\theta_{B,D^*\ell}\rvert$	<1.0
R_2	<0.3
$M^2_{\rm miss}$ (e)	< 0.0 GeV^2/c^4
$M^2_{\rm miss}$ (μ)	< 0.7 GeV^2/c^4
$\cos\theta_{D^*\ell}$	<0.0
E_{π^0}	>350 MeV
$K\pi\pi^0$ probability	>0.13

TABLE I. The cuts used in the analysis.

(3) $B \to D^{**}\ell\nu$ or $B \to D^*\pi\ell\nu$ decays producing a real D^{*+} and D^0; (4) continuum (non-$\Upsilon(4S)$ events); and (5) events in which a hadron has faked a lepton signature. With the cuts listed in Table I, we achieve a signal-to-background ratio of about 7:1 in the $D^0 \to K^-\pi^+$ channel and about 4.3:1 in the $D^0 \to K^-\pi^+\pi^0$ channel.

We start with events satisfying the standard CLEO hadronic event criteria [20]. Each event is then required to contain at least one electron candidate with momentum P_ℓ in the range 1.0 GeV/c to 2.45 GeV/c, or at least one muon candidate with momentum in the range 1.4 GeV/c to 2.45 GeV/c. The lepton direction must be in the range $|\cos\theta_\ell| < 0.71$, where θ_ℓ is the polar angle from the beam axis. Electron candidates are required to satisfy criteria based on their CsI calorimeter signature, energy loss in the drift chamber, and time-of-flight. The electron identification efficiency, about 94%, is very uniform over this momentum range. Because the uncorrelated D^{*+}–ℓ background and $B \to D^{**}\ell\nu$ decay tend to produce lower momentum leptons, we do not lower the electron momentum cut further. Muons candidates are identified by the presence of muon chamber hits after at least 5 nuclear interactions lengths of material. This criterion produces an effective minimum cut on the muon momentum at about 1.2 GeV/c; we raise the cut to 1.4 GeV/c, where the efficiency is higher. The backgrounds from hadrons faking leptons are very low, as indicated in Table II, which summarizes the backgrounds after all cuts are applied.

Continuum background is suppressed using an event shape variable R_2, equal to the ratio of the second to the zeroth Fox-Wolfram moments [21]. This quantity is required to be less than 0.3 (a value of 0 corresponds to a perfectly spherical event, whereas 1.0 corresponds to a perfectly jetlike event).

We next search for D^0 signals in the modes $D^0 \to K^-\pi^+$ and $D^0 \to K^-\pi^+\pi^0$. In the first mode, no particle identification is required for the charged kaon and pion; besides loose track quality cuts, we require only that the candidates have opposite charges and that the kaon

	$K\pi$	$K\pi\pi^0$	$K\pi + K\pi\pi^0$
Events in signal region	478 ± 22	305 ± 17	783 ± 28
Fake D^*	31 ± 11	37 ± 13	68 ± 24
$B \to D^{**}\ell\nu$	19 ± 6	12 ± 7	31 ± 13
Continuum	1 ± 1	1 ± 1	2 ± 2
Uncorrelated	9 ± 4	8 ± 3	17 ± 5
Fake leptons	5 ± 2	4 ± 2	9 ± 3
Signal	413 ± 26	243 ± 23	656 ± 23

TABLE II. The yields in the $K\pi$ and $K\pi\pi^0$ modes and the estimated background contamination of the signal.

have the same charge as the lepton. For the three-body D decay, there is more combinatorial background, so we use dE/dx information from the drift chamber to help identify the kaon. The π^0 is identified using the CsI calorimeter: the photons are required to have energies of at least 50 MeV, the π^0 mass must be within 2σ of the nominal value, and E_{π^0}, the π^0 energy in the lab frame, must be at least 350 MeV. The $D^0 \to K^-\pi^+$ candidates must have a $K^-\pi^+$ mass within 16 MeV/c^2 of the nominal D^0 value; $D^0 \to K^-\pi^+\pi^0$ candidates must have a $K^-\pi^+\pi^0$ mass within 25 MeV/c^2 of the nominal value. The D^0 candidates must have a lab-frame momentum P_{D^0} less than 2.45 GeV/c, which is close to the kinematic limit for D^*'s from B decays. This cut helps to reduce background from continuum charm production.

To further reduce the combinatorial background in reconstructing the three-body D decay, we use measurements of the $D^0 \to K^-\pi^+\pi^0$ Dalitz plot from E691 [22] to compute a weight for each $K^-\pi^+\pi^0$ combination. We require a minimum value of this weight, which selects $K^-\pi^+\pi^0$ configurations within the more highly populated regions of the $D^0 \to K^-\pi^+\pi^0$ Dalitz plot. This cut is very useful since it is essentially uncorrelated with any of the kinematic distributions that enter the form factor analysis.

We reconstruct charged D^* candidates by combining D^0's with additional charged tracks of momentum P_{π_s} at least 65 MeV/c. The charge of this pion candidate must be opposite to that of the lepton. We then compute the mass difference $\delta m = m(D^{*+}) - m(D^0)$, where D^{*+} and D^0 here denote the candidate particle combinations. Figure 2 shows the δm distributions for the $D^0 \to K^-\pi^+$ and $D^0 \to K^-\pi^+\pi^0$ channels. (These plots show the distributions after all analysis cuts are applied.) It is evident that in each channel there is very little background from fake D^*'s; such events turn out to be the largest of all the backgrounds. We select D^* candidates in both channels by requiring that δm be within 2 MeV/c^2 of the nominal value. To estimate the background from fake D^*'s we use the sideband region $0.15 < \delta m < 0.17$ GeV/c^2.

To suppress background from events in which the D^{*+} and the lepton are produced by different B's (uncorrelated background), we require the D^{*+} and the lepton to be in opposite hemispheres. If the D^{*+} and the lepton are produced in a $B \to D^*\ell\nu$ decay, they tend to be in opposite hemispheres, whereas the uncorrelated background is uniformly distributed in $\cos\theta_{D^*\ell}$, where $\theta_{D^*\ell}$ is the angle between the D^{*+} and the lepton in the lab frame.

The final step in the event selection is designed to exploit the fact that, in the decay $\bar{B}^0 \to D^{*+}\ell^-\overline{\nu}$, the kinematics of the decay must be consistent with the presence of a neutrino recoiling against the $D^{*+}\ell^-$ system. If the four-momentum of the parent B meson were exactly known, it would be possible to calculate without any approximation the four-momentum of the missing particle or particles: $p_{\rm miss} = p_B - p_{D^*} - p_\ell$. For $B \to D^*\ell\nu$, $p^2_{\rm miss} = m^2_\nu = 0$. In our case, the magnitude of the B momentum is known, but not its direction. We can estimate the missing mass squared $p^2_{\rm miss}$ using

$$\begin{aligned} p^2_{\rm miss} &= (p_B - p_{D^*\ell})^2 \\ &= m^2_B + m^2_{D^*\ell} - 2E_B E_{D^*\ell} + 2|\mathbf{p}_B||\mathbf{p}_{D^*\ell}|\cos\theta_{B,D^*\ell} \end{aligned} \tag{15}$$

where $p_{D^*\ell} = p_{D^*} + p_\ell$. Although the angle $\theta_{B,D^*\ell}$ between the B and $(D^* + \ell^-)$ momentum directions is unknown, one can neglect the last term since $|\mathbf{p}_B| \approx 330$ MeV/c is small. Thus, we define

$$M^2_{\rm miss} = m^2_B + m^2_{D^*\ell} - 2E_B E_{D^*\ell}. \tag{16}$$

The quantity $M^2_{\rm miss}$ is appealing intuitively because background from $B \to D^{**}\ell\nu$, which produces an additional pion, peaks at larger values of $M^2_{\rm miss}$ than the signal. To suppress background from $B \to D^{**}\ell\nu$ we require $M^2_{\rm miss} < 0$ for events with electrons and $M^2_{\rm miss} < 0.7$ GeV$^2/c^4$ for events with muons. The muon channel has a looser cut because the higher momentum requirement in the muon channel already removes a substantial amount of the $B \to D^{**}\ell\nu$ background. The cuts are designed to reduce this background to about the same size in the electron and muon samples.

We can also impose the condition $p^2_{\rm miss} = 0$, which is satisfied for signal events, and solve Eq. 15 for $\cos\theta_{B,D^*\ell}$. The quantity $\cos\theta_{B,D^*\ell}$ computed in this way is highly correlated with the estimated value of $M^2_{\rm miss}$, but it allows us to precisely impose the kinematic consistency condition through the requirement $|\cos\theta_{B,D^*\ell}| \leq 1$, which is satified by signal events up to small resolution effects. (The cut $M^2_{\rm miss} < 0$, used for electrons, corresponds to $\cos\theta_{B,D^*\ell} > 0$.) Figures 3 and 4 show (before cuts on either $M^2_{\rm miss}$ or $\cos\theta_{B,D^*\ell}$) the distribution of data events for this variable in the $D^0 \to K^-\pi^+$ channel, as well as the predicted distributions for backgrounds from fake D^{*+}'s and $B \to D^{**}\ell\nu$. (Other backgrounds are very small and are not shown.) The points with error bars are the data, and the solid histogram shows the sum of the Monte Carlo signal and the distributions for the background. The $\cos\theta_{B,D^*\ell}$ distribution for fake D^{*+}'s is obtained using events in the sideband region of the mass difference distribution. It is normalized by fitting the mass difference distribution and extrapolating the background shape into the peak region. The $B \to D^{**}\ell\nu$ background is modeled using Monte Carlo events distributed according to the ISGW model [1]. The overall normalization of the $B \to D^{**}\ell\nu$ background is not well known, but we can use the CLEO-II 95% C.L. limit $\mathcal{B}(B \to D^{**}\ell\nu) < 2.8\%$ [15], which is consistent with the ARGUS measurement [14], $\mathcal{B}(B \to D^{**}\ell\nu) = (2.7 \pm 0.7)\%$. Because this measurement involves several assumptions that are difficult to verify, we take the approach of minimizing the $B \to D^{**}\ell\nu$ background even though we lose a significant number of signal events.

Table II lists the estimated number of events from each background and the signal. Continuum and fake-lepton backgrounds are essentially negligible. The largest backgrounds are fake D^{*+}'s and $B \to D^{**}\ell\nu$ decays. The final sample of 783 events consists of 656 signal and 127 background events.

IV. KINEMATIC VARIABLES AND ACCEPTANCE EFFECTS.

To extract the form factors, we perform a fit to the joint distribution in the kinematic variables $\cos\theta_\ell$, $\cos\theta_V$, χ, and q^2. It is important to reconstruct these variables with the best possible resolution. The dominant source of smearing is the unknown direction of the B meson, which has velocity $\beta \approx 0.06$ in the lab frame. The effect of the B motion is especially important at high q^2, where the D^* moves slowly in the B rest frame; the boost from the B motion can then account for a substantial fraction of the observed D^* momentum.

Although there is not enough information to completely determine the direction of the B momentum vector, there are useful constraints. We have already used the known beam energy and the assumption that the $D^{*+}\ell^-$ system is recoiling against a neutrino (with no additional particles) to compute $\cos\theta_{B,D^*\ell}$, where $\theta_{B,D^*\ell}$ is the angle between $\mathbf{p}_B$ and $\mathbf{p}_{D^*\ell} = \mathbf{p}_{D^*} + \mathbf{p}_\ell$. Thus, the direction of the B meson is constrained to lie on a cone of known opening angle with respect to $\mathbf{p}_{D^*\ell}$. The azimuth of $\mathbf{p}_B$ on this cone cannot, however, be determined. Within this constraint, we consider two extreme configurations, those with the largest and smallest opening angles between $\mathbf{p}_B$ and $\mathbf{p}_{D^*}$. These configurations correspond, respectively, to the smallest and largest values of q^2 consistent with the observed four-vectors, since

$$q^2 = (p_B - p_{D^*})^2 = m_B^2 + m_{D^*}^2 - 2(E_B E_{D^*} - |\mathbf{p}_B||\mathbf{p}_{D^*}|\cos\theta_{B,D^*}). \tag{17}$$

Our method is to compute the values of q^2, $\cos\theta_\ell$, $\cos\theta_V$, and χ for each of these extreme configurations and to use the average as the estimate for each kinematic variable. Occasionally, the minimum value of q^2 will be negative, which is unphysical. In this case, we set $q^2_{\rm min} = 0$ before computing the average.

The resulting resolution in each variable is good and is significantly improved over the calculation in which the B motion is ignored. The resolutions are q^2 dependent, with typical values $\sigma(q^2) \approx 0.5$ GeV$^2/c^4$, $\sigma(\cos\theta_\ell) \approx 0.07$, $\sigma(\cos\theta_V) \approx 0.07$, $\sigma(\chi) \approx 0.24$. None of these is negligible, however, and we therefore use a fitting method that takes the smearing into account.

In addition to smearing, the fit must also take into account detector acceptance. The most important acceptance effects are the poor detection efficiency for charged pions with momenta less than about 100 MeV/c and the low-momentum cutoff for leptons. The soft-pion acceptance effect is particularly important at high q^2, where the D^* is moving slowly. The decay $D^* \to D^0\pi^+$ then produces a very low momentum pion, which is only able to reach the inner portion of the CLEO tracking volume, where there are only a few measurements of the z coordinate. Thus, to correctly measure both the q^2 and $\cos\theta_V$ distributions it is important to have good knowledge of the momentum dependence of the soft-pion detection efficiency.

The shape of the soft-pion acceptance has been measured in the data using $D^* \to D^0\pi^+$ decays produced in continuum events. The technique exploits the fact that this process conserves parity, and hence the decay-angular distribution is forward-backward symmetric in the D^* rest frame. This angular distribution translates into a range of pion momenta in the detector frame, depending on the velocity of the D^*. The observed lack of forward-backward symmetry in the pion angular distribution can therefore be traced to the fact that backward-going pions have lower momenta in the lab frame and so have a lower detection efficiency. This observation has been used to map out the soft-pion detection efficiency in data, and it has been verified that the Monte Carlo correctly models the acceptance. The range of uncertainty in the shape of the soft pion efficiency function (due to the statistical error in the study) has been included in the systematic errors on the form factors (see Table IV). Figure 5 shows the soft-pion momentum spectrum for the $D^0 \to K^-\pi^+$ channel, together with the prediction from the ISGW model for $B \to D^*\ell\nu$. This prediction, however, is not very sensitive to the details of the model.

A similar acceptance effect arises for leptons: leptons produced in the forward direction in the W rest frame are Lorentz boosted to a higher momentum than those produced in the backward direction, for a fixed value of q^2. The acceptance effect is more severe for muons than for electrons, because muon identification requires that a charged particle penetrate 5 interactions lengths of iron absorber, whereas electron identification requires that the track reach the CsI calorimeter. The electron momentum cut, $p_\ell > 1.0$ GeV/c, is actually somewhat higher than the minimum required for good electron identification, in order to suppress background from $B \to D^{**}\ell\nu$ decays and from events in which the D^* and lepton are not produced by the same B meson. The cutoff in efficiency for low-momentum leptons directly affects the distribution of $\cos\theta_\ell$, since the efficiency for backward-going leptons ($\cos\theta_\ell < 0$) is very low. (The requirement that the D^* and the lepton be in opposite hemispheres, which designed to remove background from uncorrelated D^*–lepton pairs, also reduces the $\cos\theta_\ell$ efficiency in the backward direction.) Because the lepton forward-backward asymmetry is governed by the form factor ratio R_1, this quantity is difficult to measure precisely. However, the use of the $\cos\theta_V$ vs. χ correlation provides powerful information on R_1 that compensates for the poor $\cos\theta_\ell$ acceptance.

Figure 6 shows the shape of the acceptance curves for each of the four variables in the fit. The curves are shown separately for electrons and muons, since there are substantial differences in the $\cos\theta_\ell$ acceptance. The acceptance for electrons at low values of $\cos\theta_\ell$ is better than that for muons, so events with electrons are more important for measuring R_1. The $\cos\theta_V$ acceptance falls in the forward direction because this corresponds to a backward-going charged pion from the $D^{*+} \to D^0\pi^+$ decay. Also shown are the theoretical distributions, without acceptance corrections, that result from the fit to the data. We now turn to the fitting method and the fit results.

V. FITTING METHOD

The joint distribution in q^2, $\cos\theta_\ell$, $\cos\theta_V$, and χ is fit using the unbinned maximum likelihood method. To fully incorporate detector smearing and acceptance effects, we use a Monte Carlo technique to evaluate the likelihood function. This technique was first used by Fermilab E691 [16] and has been used in several form factor analyses. We briefly describe the idea of this method below.

The likelihood of the data sample is calculated, for any given set of theoretical parameters, by computing the density of Monte Carlo events around each data point, where the Monte Carlo events are distributed according to the theoretical parameters under consideration. To avoid the need to generate separate Monte Carlo samples for every set of theoretical parameters considered by the fitter, we reweight a single Monte Carlo sample so that the weighted events give the correct density about each data point. This procedure allows us to incorporate the acceptance and smearing effects automatically, since these are well modeled by the Monte Carlo.

Thus, a single Monte Carlo sample is generated according to set of theoretical parameters, which we denote by $\hat{\mu}$. The events are passed through a GEANT simulation of the detector and are reconstructed and analyzed using the same cuts as those used for the data. The reconstructed events are distributed according to

$$F(\tilde{y};\hat{\mu}) = \int \mathcal{D}(\tilde{y},y)\Gamma(y;\hat{\mu})dy, \tag{18}$$

where $\Gamma(y;\hat{\mu})$ is the theoretical distribution and $\mathcal{D}(\tilde{y},y)$ represents the smearing and acceptance function, which in practice is computed using the Monte Carlo. The symbol $\tilde{y}$ refers to the reconstructed (observed) value of y. Let x and $\tilde{x}$ denote the true and measured quantities, but for data. For Monte Carlo events we know both y and $\tilde{y}$, but for data we know only $\tilde{x}$. To perform the maximum likelihood fit we must evaluate the function

$$ln\mathcal{L}(\mu) = \sum_{i=1}^{n}[lnF(\tilde{x}_i;\mu) - lnI(\mu)], \tag{19}$$

where $I(\mu) = \int F(\tilde{x};\mu)d\tilde{x}$ is the normalization and the sum is over all data points. First, we note that if we have a Monte Carlo sample generated according to $\hat{\mu}$ it is easy to evaluate the likelihood for that theory. Since the $\tilde{y}$ are distributed according to $F(\tilde{y};\hat{\mu})$ we can select a volume V_i centered at each observed data point, $\tilde{x}_i$, in the space of $\tilde{x}$ and count how many Monte Carlo events fall within V_i. Thus,

$$\frac{1}{N}\frac{dN}{d\tilde{x}}(\tilde{x}=\tilde{x}_i;\mu=\hat{\mu}) = \frac{F(\tilde{x}_i;\hat{\mu})}{I(\hat{\mu})} = \frac{\text{Number of } \{\tilde{y}_j\} \text{ in } V_i}{V_i \times (\text{Number of reconstructed MC events}).} \tag{20}$$

To calculate the likelihood function for a different value of the theoretical parameters μ without generating a new Monte Carlo sample, we assign a weight $W(y_j;\mu) = \Gamma(y_j;\mu)/\Gamma(y_j;\hat{\mu})$ to each Monte Carlo event $(\tilde{y}_j, y_j)$. The Monte Carlo events with weight $W(y;\mu)$ are distributed according to $F(\tilde{y};\mu)$. The main point is that the effects of the acceptance and the smearing for any parameter set μ can be evaluated simply by re-weighting MC events distributed according to a parameter set $\hat{\mu}$, as long as the set $\hat{\mu}$ populates all of the phase space.

If we have a set of n data events and m MC events we can write the log-likelihood as

$$ln\mathcal{L}(\mu) = \sum_{i=1}^{n} ln\left[\frac{\sum_{\tilde{y}_j \text{ in } V_i} W(y_j;\mu)}{C(\mu)V_i}\right], \tag{21}$$

where V_i is the volume centered around $\tilde{x}_i$ and $C(\mu) = \sum_{j=1}^{m} W(y_j;\mu)$ is the normalization of the weighted MC sample. When $\mu = \hat{\mu}$ the expression simplifies to the case above.

In our fits, there are four channels, since there are two lepton types and two D^0 decay modes. In calculating the likelihood function for a given event, we use the Monte Carlo sample generated for the channel in which the event was reconstructed.

The largest background in the analysis, which is less than 10% of the signal, is due to the combinatoric background under the $D^* - D$ mass difference peak. A term is included in the fit to represent this fake D^{*+} background, whose normalization is determined from the

$D^* - D$ sideband. The shapes of the distributions for the kinematic variables are obtained with Monte Carlo, since large samples are required to evaluate the likelihood function. However, we have compared the kinematic distributions predicted from Monte Carlo with those measured from the sideband and have found good agreement. This comparison is shown in Figure 7.

The background from the uncorrelated D^*–lepton events (see section III) is also incorporated into the fit as an additional component of the fitting function. Its normalization is measured from the data. The $B \to D^{**}\ell\nu$ background is treated differently. A term is not included in the fitting function, but we use Monte Carlo events to evaluate a systematic error that could be caused by omitting this background in the fit.

VI. FIT RESULTS

Figure 8 shows the data distributions for the four fit variables after all cuts are applied. The data shown are the combined $D^0 \to K^-\pi^+$ and $D^0 \to K^-\pi^+\pi^0$ modes and include both electrons and muons. The dotted line in each histogram shows the fit result, which agrees well with the data in all variables. The distribution for the combined background from fake D^{*+} and uncorrelated D^{*+}–lepton events is shown as a dashed line. These background distributions do not show any dramatic behavior. In interpreting these plots, it is important to remember the effects of acceptance, especially in parts of phase space in which either the pion from D^{*+} decay or the lepton has low momentum. (These acceptance effects were shown in Fig. 6 for the $D^0 \to K^-\pi^+$ channel and are similar for the $D^0 \to K^-\pi^+\pi^0$ channel.)

The fit makes use of much more information than is seen in these simple projections. Figures 9 and 10 show some of this information. The scatterplot of $\cos\theta_V$ vs. q^2 shows a strong correlation between these variables, which can be easily understood. At low q^2, the lepton and neutrino are parallel, forcing the W, and hence the D^{*+}, to have helicity zero. As a result, $\cos\theta_V$ is distributed as $\cos^2\theta_V$, which produces the large depleted region (except for large $|\cos\theta_V|$) on the left-hand side of the scatterplot. As q^2 increases, the helicity zero component of the D^{*+} no longer dominates. Since either helicity $+1$ or -1 produces a $\sin^2\theta_V$ distribution (see Eq. 1), the density in the central region of the scatterplot increases. This progression is also seen in the two slices made for the lower and higher half-ranges of q^2. The figure also shows the scatterplot that is expected for the measured fit parameters, which agrees well with what is observed.

Figure 10 shows an interesting correlation between $\cos\theta_V$ and χ. This correlation is produced by two interference terms in the amplitude, and it clearly shows the parity-violating nature of the decay. The pattern evident in the scatterplot is the result of summing the last two terms in Eq. 1 and integrating over $\cos\theta_\ell$. One then obtains a term proportional to $(H_+(q^2) - H_-(q^2))H_0(q^2)$. The difference $H_+ - H_-$ is large and negative because in the decay $\bar{B}^0 \to D^{*+}\ell^-\overline{\nu}$ the daughter c-quark has a higher probability to have helicity $-1/2$ than helicity $+1/2$. This difference in turn results in a higher probability for the D^{*+} and the W to have helicity -1 than $+1$. (In $\bar{B}$ decays, the effect is reversed, but the resulting angular distribution is the same because the lepton helicity also changes.) The scatterplot in Fig. 10 shows two depleted regions in the lower left and upper right; if the coupling at the W vertices were $(V \mp A) \times (V \pm A)$ these regions would be enhanced rather than depleted. The χ distributions, made separately for low and high values of $\cos\theta_V$, show this effect

Fit Parameters	
R_1	$1.30 \pm 0.36 \pm 0.16$
R_2	$0.64 \pm 0.26 \pm 0.12$
ρ^2	$1.01 \pm 0.15 \pm 0.09$
Correlation Coefficients	
$C(R_1 R_2)$	-0.83
$C(R_1 \rho^2)$	0.63
$C(R_2 \rho^2)$	-0.82

TABLE III. The preliminary result of the three parameter fit. The first error is statistical the second is systematic.

strongly. The positive slope in χ for $\cos\theta_V < 0$ and the negative slope for $\cos\theta_V > 0$ are consistent with the $(V-A)(V-A)$ coupling at the two vertices but would be reversed for a $(V \mp A)(V \pm A)$ coupling.

All observed distributions are well described by the fit. The preliminary values of R_1, R_2, and ρ^2 that we obtain are given in Table III. Because there are large correlations among their errors, we also give the off-diagonal terms of the correlation matrix.

The systematic errors on the fit results are given in Table IV. The error due to the uncertainty in the slow pion efficiency as a function of momentum is evaluated by reweighting the Monte Carlo events according to modified soft-pion efficiency functions. This function, which is measured using data as discussed in section IV, is modified according to the 1σ uncertainty on the parameters describing the shape of the curve.

The uncertainty due to Monte Carlo statistics arises from the finite size of the sample used to calculate the likelihood function, and is determined by performing fits using Monte Carlo samples of different sizes. The finite volume error is the uncertainty associated with the finite volumes used around each data point in calculating the likelihood. Such volumes must be sufficiently small to be sensitive to the variation in the distributions, but they cannot be so small that there are no Monte Carlo events within them. Thus, the number of generated Monte Carlo events is the limiting factor in reducing the volume size. We have generated a sample of 3.5 million GEANT events in order to keep our volume sizes small. The large number of events required is due to the fact that the fit is performed in four dimensions and the detection efficiency in the $D^0 \to K^-\pi^+\pi^0$ mode is low.

The uncertainty from the $B \to D^{**}\ell\nu$ background is calculated using a Monte Carlo sample generated according to the ISGW model. Events from this background sample are added to the data, and the effect on the fit parameters is determined. The mean shift in the fit parameters over many experiments of this type is very small; we take the root-mean-square shift as the systematic error.

The uncertainty associated with the lepton efficiency as a function of momentum is evaluated using the same weighting procedure as we use to determine the effect of the uncertainty on the shape of the soft-pion efficiency function.

Our fits include the uncorrelated D^{*+}–lepton background in the fitting function. We also

	R_1	R_2	ρ^2
Slow pion eff.	0.01	0.01	0.04
MC statistics	0.06	0.04	0.03
Finite volumes	0.08	0.08	0.05
$B \to D^{**}\ell\nu$	0.08	0.04	0.04
Lepton eff.	0.02	0.02	0.01
Uncorr. Bkgrnd.	0.08	0.03	0.01
δm-sideband	0.06	0.05	0.01
δm eff.	0.01	0.01	0.02
Sum	0.16	0.12	0.09

TABLE IV. The estimated systematic errors.

perform the fit without this background and take as our systematic error the full shift seen in the resulting fit parameters. The δm sideband error is the uncertainty associated with the fake D^* events. This error is determined by allowing the amount of this background to vary by $\pm 40\%$. Finally, the δm error is the uncertainty associated with the efficiency of our $\delta m = M(D^{*+}) - M(D^0)$ cut as a function of q^2. Because this cut is rather tight ($\approx 2\sigma$), incorrect modeling of the efficiency could introduce an error in measuring the q^2 distribution.

The values of R_1 and R_2 obtained from the three-parameter fit agree within errors with the predictions of Neubert [10], $R_1 = 1.3$ and $R_2 = 0.8$. The value of the slope, ρ^2, is within the range expected from lattice QCD or QCD sum rule calculations [4–6,10].

	$\bar{A}_{\rm FB}$	$\bar{A}_{\rm pol}$
ARGUS [14]	$0.20 \pm 0.08 \pm 0.06$	$1.1 \pm 0.4 \pm 0.2$
CLEO [18,19]	$0.14 \pm 0.06 \pm 0.03$	$0.65 \pm 0.66 \pm 0.25$
	$p_\ell > 1$ GeV/c	$p_\ell > 1.4$ GeV/c
CLEO-II (This measurement)	$0.209 \pm 0.034 \pm 0.015$	$1.48 \pm 0.32 \pm 0.14$
HQET [10] ($\rho^2 = 1.0$)	0.22	1.37

TABLE V. Comparison of $\bar{A}_{\rm FB}$ and $\bar{A}_{\rm pol}$ from different experiments. The earlier CLEO measurements quote the observed asymmetry and polarization for the lepton momentum cut given in the table. The ARGUS results were obtained using models to extrapolate over the full lepton-momentum range and can therefore be directly compared to this measurement and the theoretical prediction based on HQET.

To compare with previous measurements of the lepton forward-backward asymmetry, $\bar{A}_{\rm FB}$, and the D^* polarization, $\bar{A}_{\rm pol}$, we calculate these quantities from the result of the three parameter fit. Table V compares our values of $\bar{A}_{\rm FB}$ and $\bar{A}_{\rm pol}$ with previous measurements.

ρ^2	R_1	R_2	$C(R_1R_2)$
0.50	$0.77 \pm 0.21 \pm 0.16$	$1.11 \pm 0.10 \pm 0.10$	-0.67
0.75	$0.99 \pm 0.24 \pm 0.16$	$0.93 \pm 0.12 \pm 0.10$	-0.68
1.00	$1.29 \pm 0.27 \pm 0.16$	$0.65 \pm 0.15 \pm 0.10$	-0.73
1.25	$1.75 \pm 0.34 \pm 0.17$	$0.20 \pm 0.20 \pm 0.11$	-0.77

TABLE VI. The preliminary results of the two parameter fits for different slopes, ρ^2. The first error is statistical and the second is systematic. The correlation, $C(R_1R_2)$, between the errors on R_1 and R_2 is strong.

We have also performed a series of two-parameter fits for R_1 and R_2 in which ρ^2 is fixed to the values 0.50, 0.75, 1.0, and 1.25. These fits are analogous to those performed in studies of $D \to K^*\ell^+\nu$, where the pole masses are fixed. If lattice QCD calculations or other methods are able to reliably determine the value of ρ^2, one would then be able to significantly improve the errors on R_1 and R_2, as shown in Table VI.

VII. CONCLUSIONS

We have measured the form factors for the process $\bar{B}^0 \to D^{*+}\ell^-\overline{\nu}$ using an unbinned maximum likelihood fit. Three parameters are determined from the fit, two form factor ratios R_1 and R_2, and the form factor slope ρ^2. The ratios R_1 and R_2 differ somewhat from the traditional definitions used in D semileptonic decays in that their relative q^2 dependence is consistent with constraints from heavy quark symmetry. The q^2 dependence of each of the three form factors is assumed to be related by heavy quark effective theory to the Isgur-Wise function $\xi(q^2)$, which we take to be a linear function of q^2: $\xi(w) = 1 - \rho^2(w-1)$, where w is defined in Eq. 4.

With these assumptions, we obtain the preliminary form factor ratios $R_1 = 1.30 \pm 0.36 \pm 0.16$ and $R_2 = 0.64 \pm 0.26 \pm 0.12$, which can be compared with the heavy quark symmetry limit of $R_1 = R_2 = 1$. Our values agree well with the predictions of Neubert, $R_1 \approx 1.3$ and $R_2 \approx 0.8$, which include the estimated symmetry-breaking corrections. The errors on our measurements are highly correlated, as discussed in the previous section. In the same fit, we determine the slope of the Isgur-Wise function to be $\rho^2 = 1.01 \pm 0.15 \pm 0.09$. This value is consistent with the range 0.5 to 2.0 expected from calculations using lattice QCD [4–6] and QCD sum rules [7–10].

The comparison of this measurement of ρ^2 with that from the CLEO-II V_{cb} measurement [15] using $B \to D^*\ell\nu$ requires some care. That measurement uses a standard procedure in which the $d\Gamma/dq^2$ distribution is fit to a function that assumes $R_1 = R_2 = 1$. For this reason, Neubert refers to the slope parameter obtained from the $d\Gamma/dq^2$ fit as $\hat{\rho}^2$. His prediction for the relationship between ρ^2 and $\hat{\rho}^2$ is given by

$$\rho^2 \approx \hat{\rho}^2 + 0.09. \tag{22}$$

(The difference between ρ^2 and $\hat{\rho}^2$ depends on the values of R_1 and R_2.) The CLEO-II value of $\hat{\rho}^2$ is $0.84 \pm 0.13 \pm 0.08$, which would correspond to a value of ρ^2 around 0.93. Thus, the CLEO-II ρ^2 and $\hat{\rho}^2$ measurements appear to be consistent. Both are lower than the ARGUS measurements [14].

Our method for determining the $B \to D^* \ell \nu$ form factors is significantly different from previous studies. Earlier measurements have fit for at most two of the three parameters in our fit. Because of our large data sample and because we use the powerful information in the correlations among all the kinematic variables, we are able to fit simultaneously for all three parameters. In the previous CLEO-II measurement [18], the lepton forward-backward asymmetry $\bar{A}_{\rm FB}$ (see Eq. 13) was measured, and the form factors were extracted by performing a χ^2 fit to $\bar{A}_{\rm FB}$ and to both ARGUS and CLEO measurements of $\bar{A}_{\rm pol}$ and $d\Gamma/dq^2$. In that study, the q^2 dependence of the form factors was fixed. In the ARGUS measurement [14], the quantities $\bar{A}_{\rm FB}$ and $\bar{A}_{\rm pol}$ are quoted but not the form factors. In studies [14,15] of the $d\Gamma/dq^2$ distribution that are used to determine $|V_{cb}|$, a slope is determined that is closely related to ρ^2. However, these measurements assume the heavy-quark symmetry limit, $R_1 = R_2 = 1$.

One of the important results of our new fit is that the corrections to the heavy-quark symmetry limit do indeed appear to be fairly small. This result provides confidence in the use of heavy-quark symmetry as a starting point for the extraction of $|V_{cb}|$ from $B \to D^* \ell \nu$. Although our study is more general than previous ones, we have still made the important assumption that the q^2 dependence of each of the three form factors can be related to a single function (the Isgur-Wise function). Substantially more data will be required before one can allow each of the three form factors to have a separate dependence on q^2 in the fit.

We also observe a large-parity violating effect produced by the interference terms in the decay amplitude, which indicates a large difference in the amplitude for producing the W in helicity $+1$ and -1 states. This correlation helps to improve our measurement of R_1 and has not previously been used. The correlation is consistent with $(V-A)$ couplings at both W vertices.

Finally, we have performed a series of two-parameter fits in which the form-factor slope ρ^2 is fixed to a series of values within the generally expected range for this quantity. Such fits lead to significantly improved errors on R_1 and R_2.

ACKNOWLEDGEMENTS

We gratefully acknowledge the effort of the CESR staff in providing us with excellent luminosity and running conditions. J.P.A. and P.S.D. thank the PYI program of the NSF, I.P.J.S. thanks the YI program of the NSF, G.E. thanks the Heisenberg Foundation, K.K.G., I.P.J.S., and T.S. thank the TNRLC, K.K.G., H.N.N., J.D.R., T.S. and H.Y. thank the OJI program of DOE and P.R. thanks the A.P. Sloan Foundation for support. This work was supported by the National Science Foundation, the U.S. Dept. of Energy and the Natural Sciences and Engineering Research Council of Canada.

REFERENCES

[1] N. Isgur, D. Scora, B. Grinstein, and M. Wise, Phys. Rev. D **39**, 799 (1989).

[2] J. G. Körner and G. A. Schuler, Z. Phys. C **38**, 511 (1988); Z. Phys. C **46**, 93 (1990).

[3] M. Bauer and M. Wirbel, Z. Phys. C **42**, 671 (1989).

[4] S. P. Booth *et al.* (UKQCD), Phys. Rev. Lett. **72**, 462 (1994).

[5] C. Bernard, Y. Shen, and A. Soni, Phys. Lett. B **317**, 164 (1993).

[6] J. Mandula and M. Ogilvie, Nucl. Phys. B (Proc Suppl.) **26**, 459 (1992).

[7] B. Blok and M. Shifman, Phys. Rev. **D** 47, 2949 (1993).

[8] M. B. Voloshin, Phys. Rev. D **46**, 3062 (1992).

[9] J. D. Bjorken, in Gauge Bosons and Heavy Quarks, Proceedings of the 18th SLAC Summer Institute of Particle Physics, Stanford, CA, 1990, ed. by J. F. Hawthorne (SLAC Report 278), p. 167.

[10] M. Neubert, *Heavy Quark Symmetry*, SLAC–PUB–6263, June 1993, to appear in Physics Reports.

[11] N. Isgur and M.B. Wise, Phys. Lett. B **232**, 113 (1989); **237**, 527 (1990); H. Georgi, Phys. Lett. B **240**, 447 (1990).

[12] M. E. Luke, Phys. Lett. B **252**, 447 (1990).

[13] M. Neubert, Phys. Lett. B **264**, 455 (1991).

[14] H. Albrecht *et al.* (ARGUS), Z. Phys. C **57**, 533 (1993).

[15] B. Barish *et al.* (CLEO), *Measurement of the* $B \to D^*\ell\nu$ *Branching Fractions and* $|V_{cb}|$, ICHEP94 Ref. GLS0251, CLNS 94/1285.

[16] D.M. Schmidt, R.M. Morrison, and M. Witherell, Nucl. Instrum. Methods A **328**, 547 (1993).

[17] Y. Kubota *et al.* (CLEO), Nucl. Instrum. Methods A **320**, 66 (1992).

[18] S. Sanghera *et al.* (CLEO), Phys. Rev. D **47**, 791 (1993).

[19] D. Bortoletto *et al.* (CLEO), Phys. Rev. Lett. **63**, 1667 (1989).

[20] Hadronic events must have at least 3 charged tracks originating near the interaction point, and the total visible energy of the event must be greater than $0.15E_{\rm CM}$, where $E_{\rm CM}$ is the center-of-mass energy.

[21] G. Fox and S. Wolfram, Phys. Rev. Lett. **41,** 1581 (1978).

[22] J.C. Anjos *et al.* (E691), Phys. Rev. D **48**, 56 (1993).

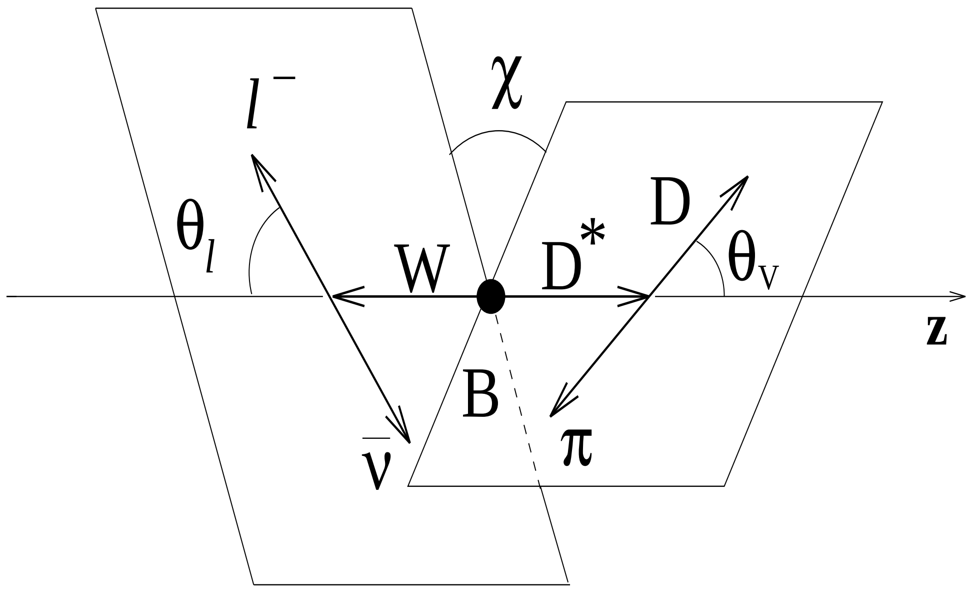

FIG. 1. Definition of the angles $\cos\theta_\ell$, $\cos\theta_V$, χ. The polar angles θ_ℓ and θ_V are defined in the rest frames of the virtual W and the D^*, respectively, and χ is the azimuthal angle between the projections of the lepton and D momentum vectors in the plane perpendicular to z.

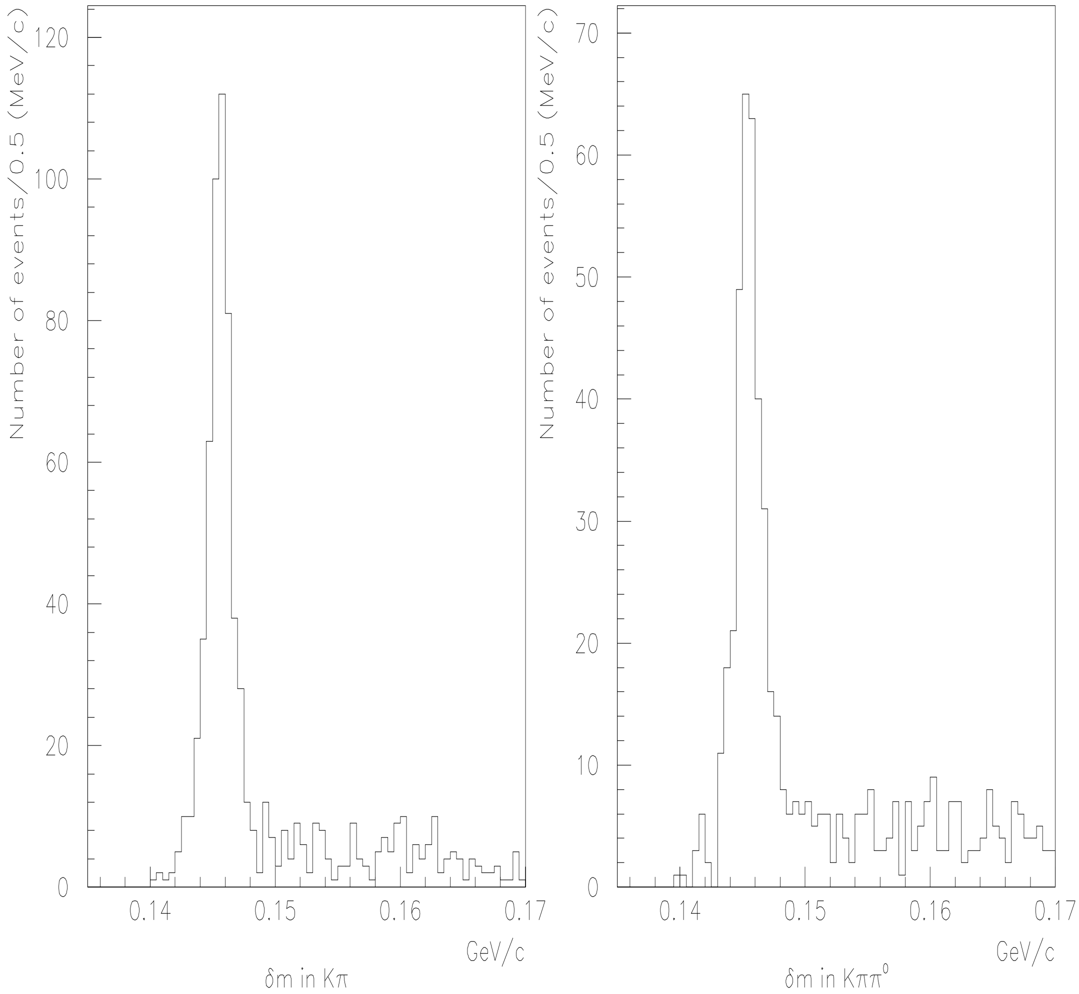

FIG. 2. The distribution of $\delta m = M(D^{*+}) - M(D^0)$ for $D^0 \to K^-\pi^+$ candidates (left) and $D^0 \to K^-\pi^+\pi^0$ candidates (right) after all analysis cuts except the δm cut.

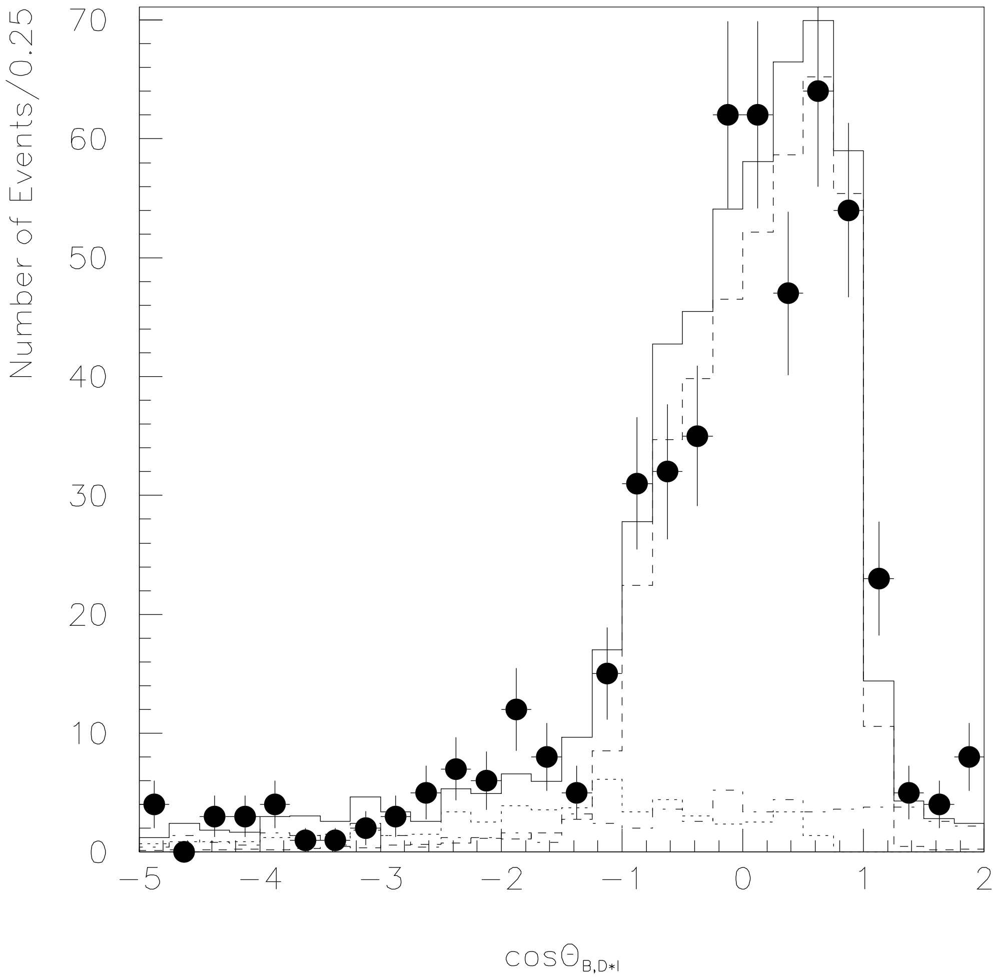

FIG. 3. The distribution of $\cos\theta_{B,D^*\ell}$ for $D^0 \to K^-\pi^+$ events with electrons. The points with error bars are the data, the dashed line is a signal shape from ISGW Monte Carlo, the dot-dashed line is the fake D^* background, the dotted line is $B \to D^{**}\ell\nu$ (simulated with ISGW Monte Carlo), and the solid histogram is the sum of the absolutely normalized backgrounds plus the Monte Carlo signal shape normalized to give the correct total number of events.

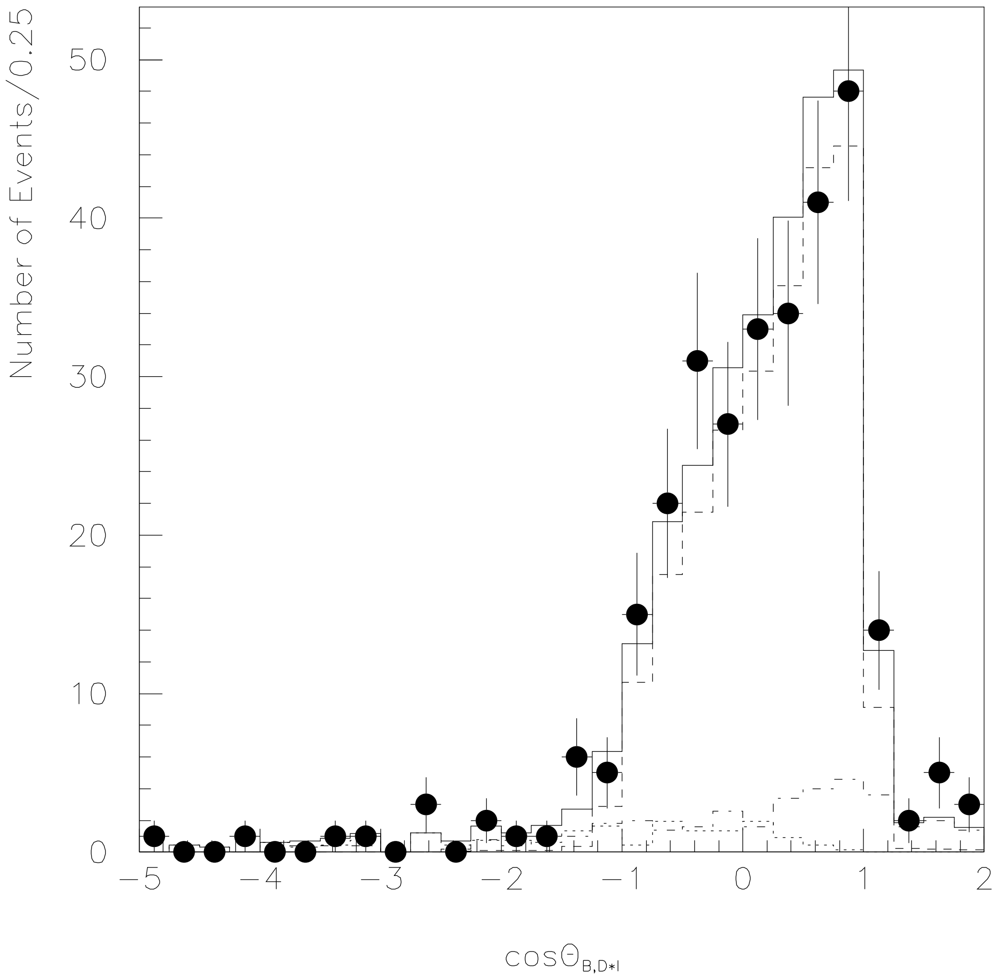

FIG. 4. The distribution of $\cos\theta_{B,D^*\ell}$ for $D^0 \to K^-\pi^+$ events with muons. The points with error bars are the data, the dashed line is a signal shape from ISGW Monte Carlo, the dot-dashed line is the fake D^{*+} background, the dotted line is $B \to D^{**}\ell\nu$ (simulated with ISGW Monte Carlo), and the histogram is the sum of the absolutely normalized backgrounds plus the Monte Carlo signal shape normalized to give the correct total number of events.

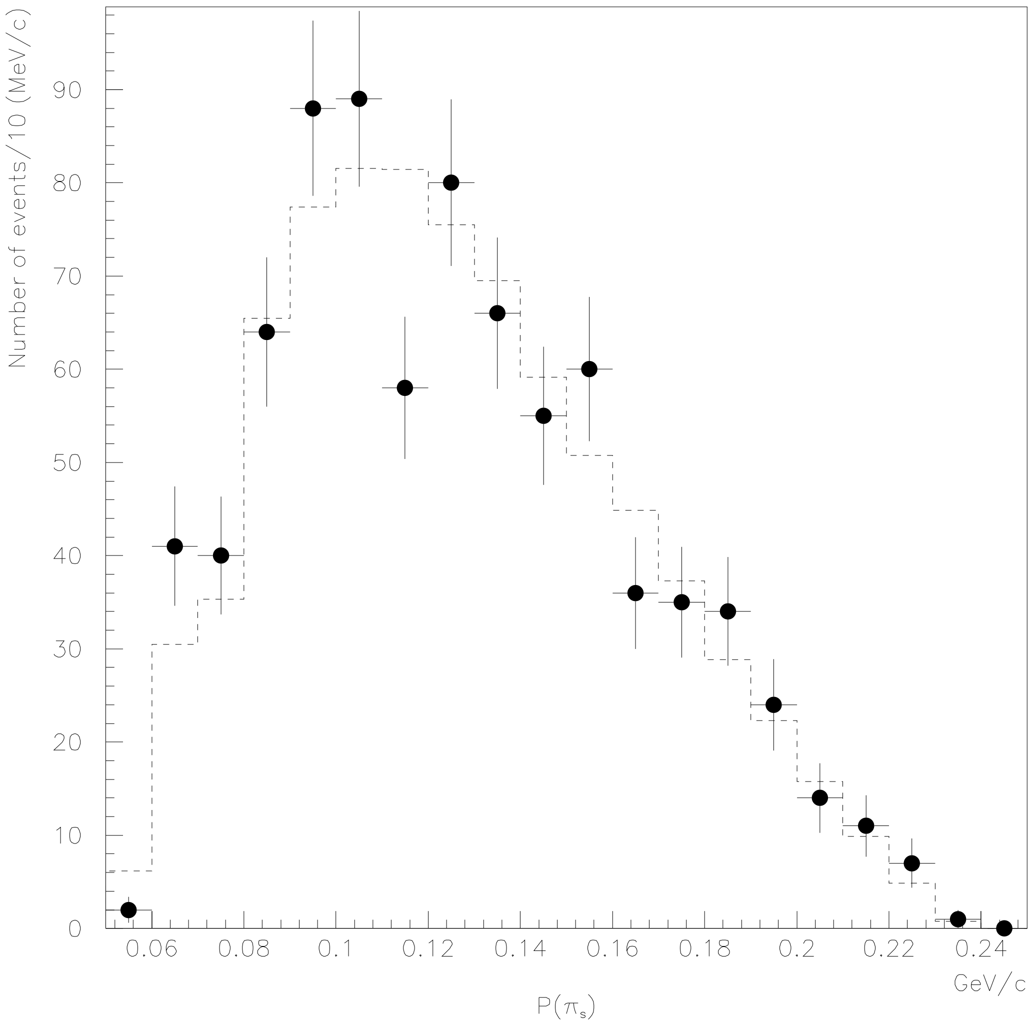

FIG. 5. The momentum distribution for soft pions from $\bar{B}^0 \to D^{*+}\ell^-\overline{\nu}$, $D^{*+} \to D^0\pi^+$. The points with error bars are data and the histogram is the expected distribution for the signal, as predicted by the ISGW Monte Carlo.

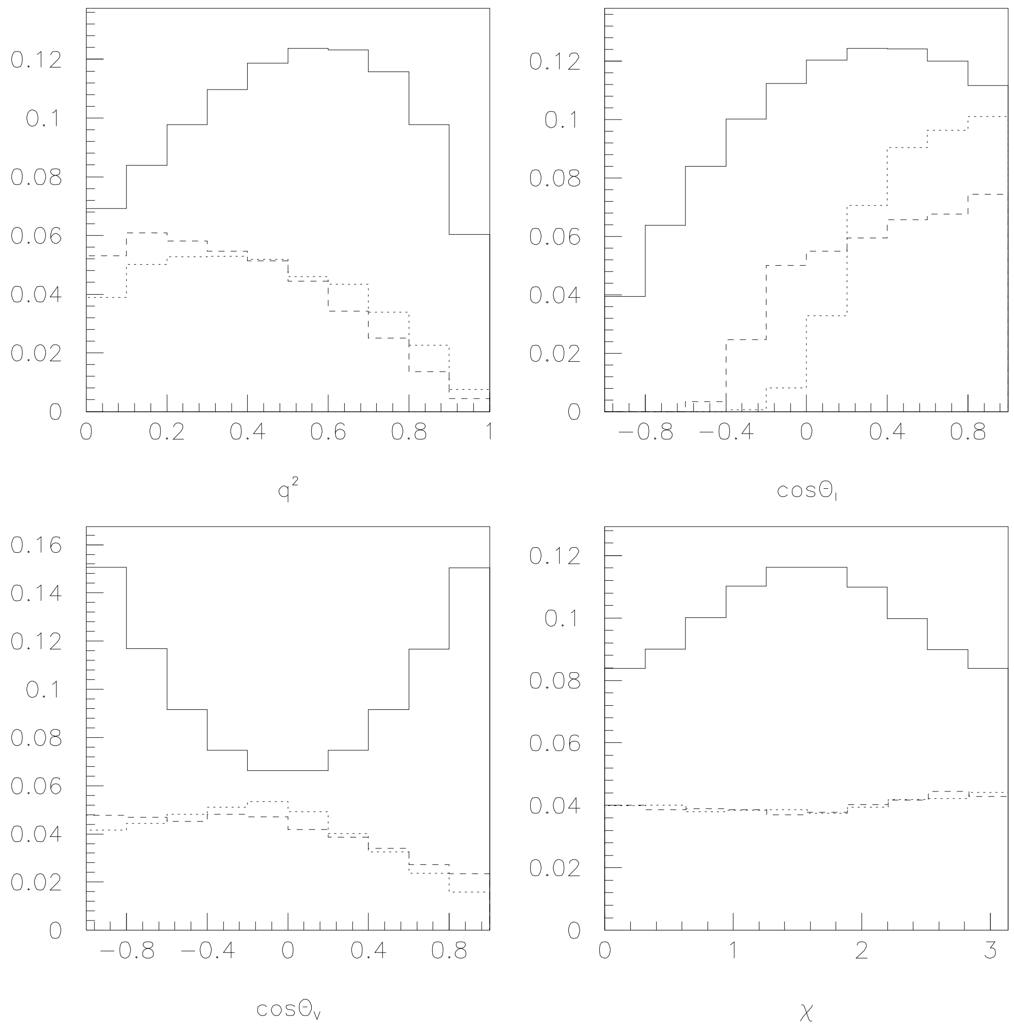

FIG. 6. The theoretical distributions that correspond to the measured values of R_1, R_2, and ρ^2, together with the shapes of the acceptance curves for each variable. The dashed line is for the electron channel in $D^0 \to K^-\pi^+$, and the dotted line is for the muon channel in $D^0 \to K^-\pi^+$. Only the shapes of the acceptance curves are meaningful in this plot, since they are each normalized to unit area. Note that the electrons have a better acceptance in $\cos\theta_\ell$, because the electron momentum cut is lower than that for muons.

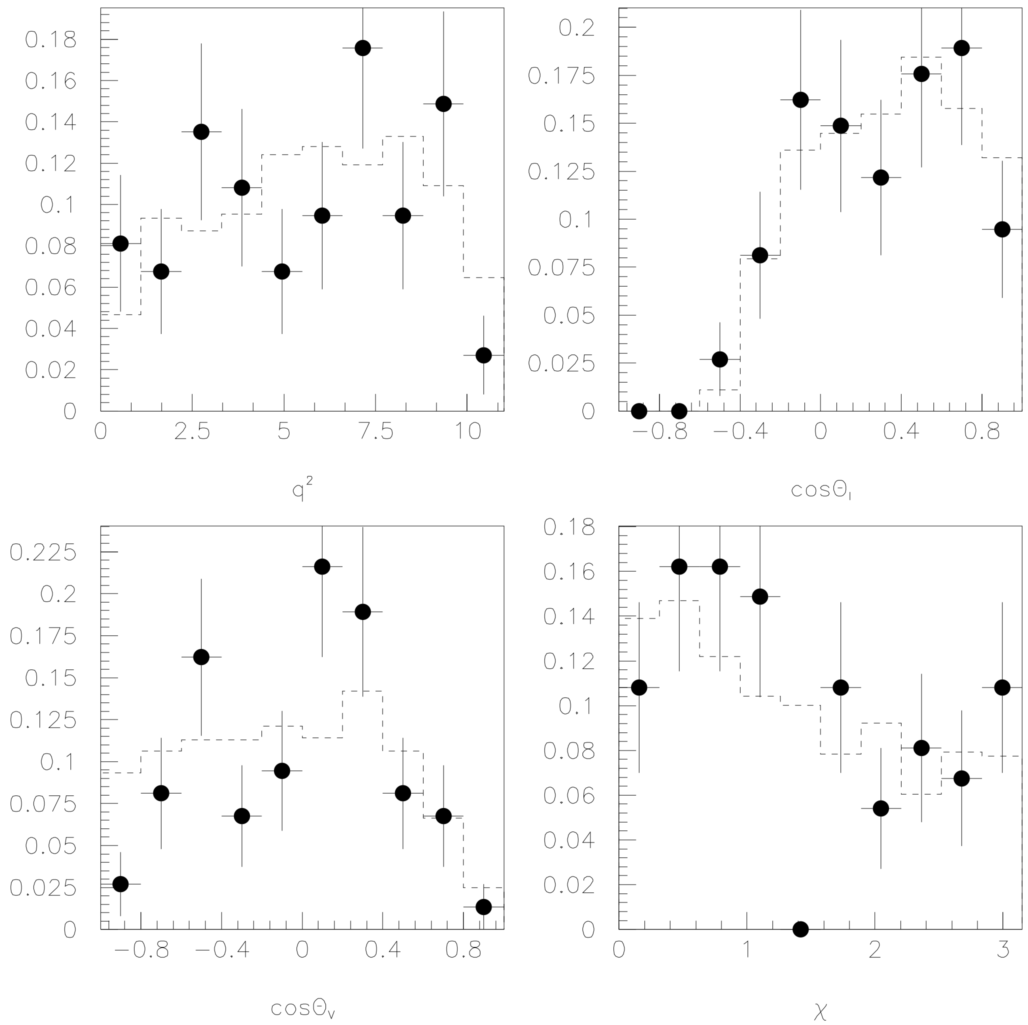

FIG. 7. Distributions of the four variables used in the fit for the combinatorial D^{*+} background (fake D^{*+}'s), which is the largest background component. The points with error bars are the data (sideband in $\delta m = M(D^{*+}) - M(D^0)$), and the histogram is the prediction of $\Upsilon(4S) \to B\bar{B}$ Monte Carlo.

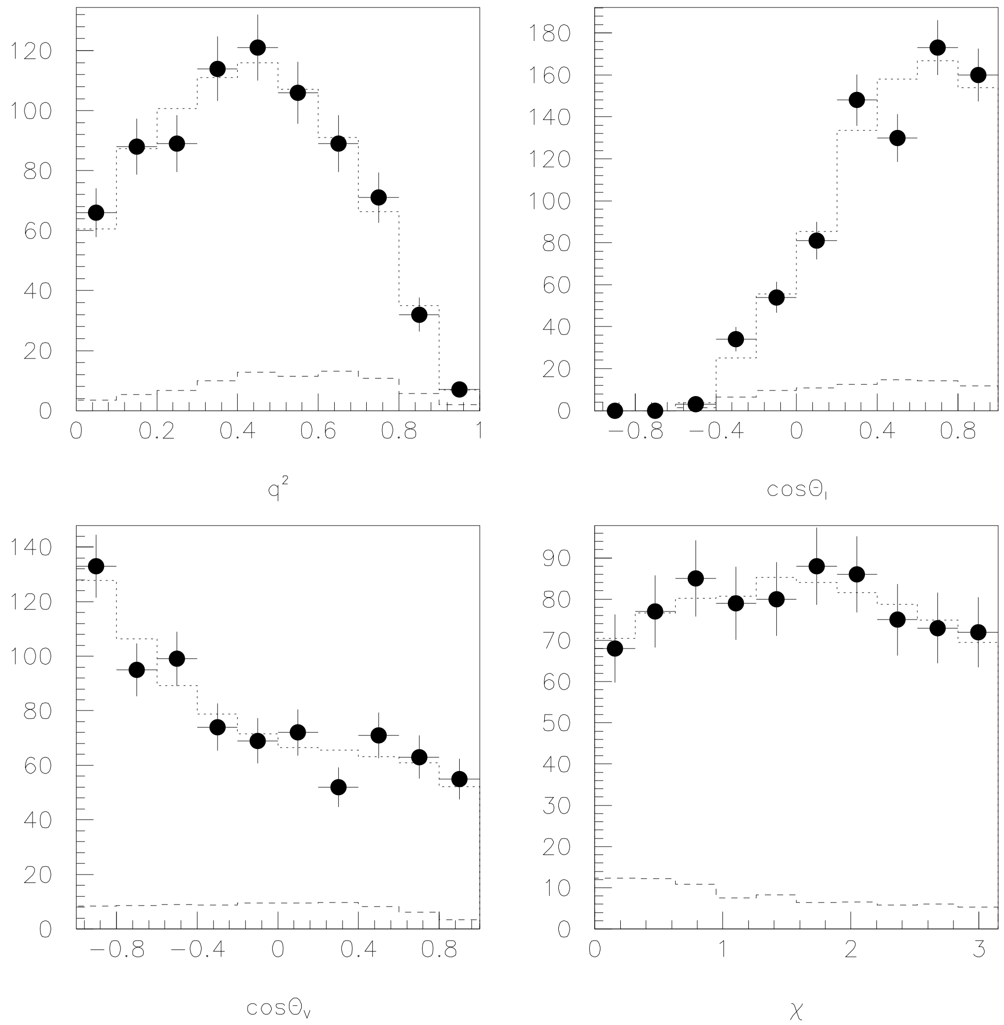

FIG. 8. The distributions of the four variables used in the fit after all cuts. The points with error bars are the data, and the dotted histogram shows the result of the fit. The dashed line shows the contribution of the two backgrounds included in the fit: fake D^{*+}'s and uncorrelated D^{*+}–lepton pairs. These histograms include both $D^0 \to K^-\pi^+$ and $D^0 \to K^-\pi^+\pi^0$ channels, electrons and muons.

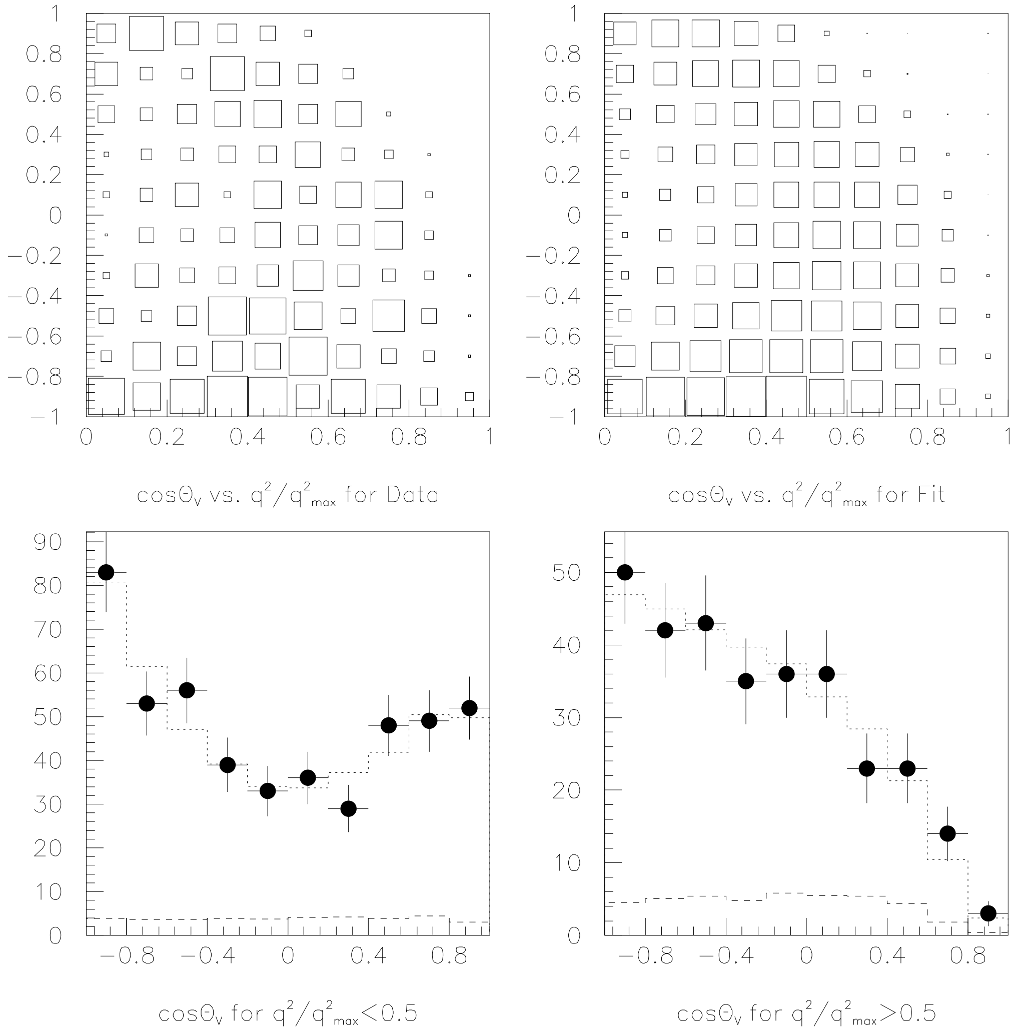

FIG. 9. The correlation between the variables q^2 and $\cos\theta_V$ as seen in the data (upper left) and fit (upper right). The lower left histogram shows the slice of $\cos\theta_V$ for $q^2/q^2_{\rm max} < 0.5$ and the lower right shows $\cos\theta_V$ for $q^2/q^2_{\rm max} > 0.5$. The dotted lines in the histograms show the result of the fit, and the dashed lines show the background from fake D^{*+}'s and uncorrelated D^{*+}-lepton events. At low q^2, the longitudinal component of the D^* dominates. At $q^2_{\rm max}$, the D^* is unpolarized.

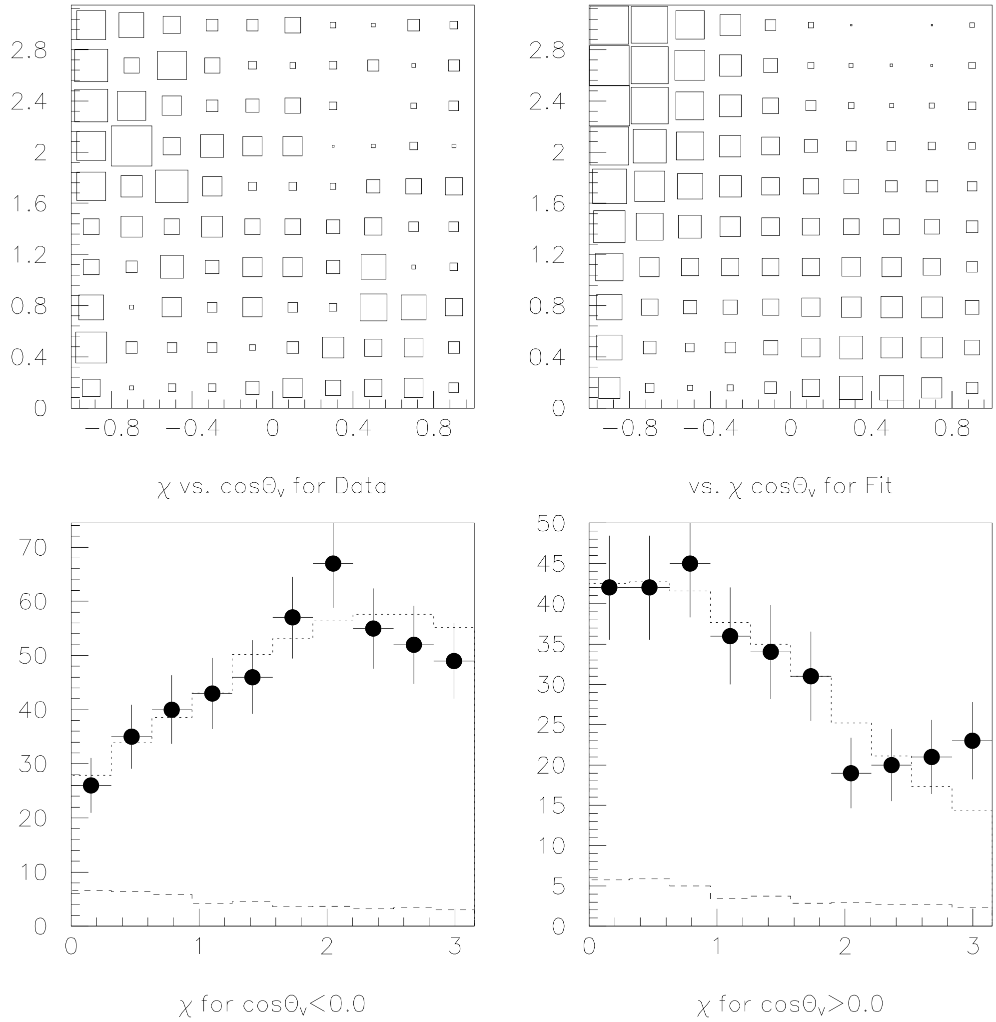

FIG. 10. The correlation between the variables χ and $\cos\theta_V$, as seen in the data (upper left) and fit (upper right). The lower-left histogram shows the slice of χ for $\cos\theta_V < 0.0$, and the lower-right shows χ for $\cos\theta_V > 0.0$ The dotted lines in the histograms show the result of the fit, and the dashed lines show the background from fake D^{*+}'s and uncorrelated D^{*+}-lepton events. The shift from positive to negative slope in these histograms is characteristic of the $(V-A)\times(V-A)$ coupling, and the pattern would be reversed if one of the couplings were changed to $V+A$.